Investigating the Low-Mass Stellar Initial Mass Function in Draco

A THESIS
SUBMITTED TO THE FACULTY OF THE GRADUATE SCHOOL
OF THE UNIVERSITY OF MINNESOTA
BY

Seyed Soroush Sotoudeh

IN PARTIAL FULFILLMENT OF THE REQUIREMENTS
FOR THE DEGREE OF
MASTER OF SCIENCE

Evan D. Skillman, Advisor

May, 2016

Acknowledgements

I would like to express my special appreciation and gratitude to my advisor, Professor Evan D. Skillman of the School of Physics and Astronomy at the University of Minnesota. Prof. Skillman has always been an excellent mentor for me and he gave me the unique opportunity and support to work in the field that I truly love. I appreciate his guidance and generous contribution of knowledge and experience.

I would also like to thank my committee members, Professor Robert Lysak, Professor Liliya L. R. Williams and my advisor for serving as my committee members.

Next, I would like to thank Dr. Dan Weisz and Dr. Andy Dolphin for being generous in sharing their knowledge and time with me and for their great help and valuable comments throughout my research.

And finally, I would like to thank all my family members. Words cannot express my thankfulness. Without their love, support and sacrifices, none of this could have happened.

Dedication

I would like to dedicate my thesis to my dear parents, Mohammad Rahmat Sotoudeh and Sophia Mohammadzadeh, and my dear sister, Mahsa Sotoudeh, without whom this accomplishment would not have ever been possible.

Abstract

We present new analysis of the low-mass stellar initial mass function ($\sim 0.4-0.8 M_{\odot}$) in the Local Group dwarf spheroidal galaxy, Draco. Using archival HST/ACS and WFC3 optical imaging, we construct deep color-magnitude (CMD) diagrams in 3 different felds at 3 different galactocentric radii and measure the IMF by modeling the resolved lower main sequence. We model the optical color-magnitude diagrams of each feld assuming two different IMF models (power-law, log-normal), five different stellar evolution libraries (Padova, BaSTI, Dartmouth, Victoria, PARSEC), and a binary star model. For a single-sloped power-law IMF model, we find that the IMF slope steepens by up to 0.7 dex for radii between 150 and 300pc, while the binary fraction remains approximately constant. The absolute values of the IMF slopes at any radius depend strongly on the adopted stellar models, suggesting that current knowledge of the lower-main sequence stars is uncertain. In fact, utilizing different stellar models has resulted in up to 0.67 dex difference in the IMF slope. All fields show more consistent log-normal parameters, which are also in reasonable agreement with values for a standard Chabrier IMF. However, there are large degeneracies between the characteristic mass and dispersion of the log-normal, that can only be reduced with data that extends to lower stellar masses.

Contents

List of Tables

List of Figures

Chapter 1

Introduction

The IMF is fundamental to most of the astrophysical calculations, studies of galaxies and stellar populations and is originated from the star formation theory. So, having a better understanding of the stellar IMF could provide us with deeper insights into the star formation theory. It can also help us to understand how the distribution of stellar masses is related to processes such as turbulence, gravitational fragmentation of clouds, accretion in dense cores, and ejection of low-mass objects [1] .

1.1 Functional Forms

The IMF was first introduced by Salpeter [1955] and many other functional forms have been proposed for it so far. In his 1955 paper, E. Salpeter introduced a power-law IMF of the form,

$$\Phi(\log m) = dN/d\log m \propto m^{-\Gamma} \tag{1.1}$$

where m is the mass of a star and N is the number of stars in some logarithmic mass range $logm + dlogm$. Salpeter's studies revealed a Γ of 1.35 for stars down to $0.4M_{\odot}$. Most of the recent studies of the Galaxy suggest other forms for the IMF on the low-mass end. As mentioned previously, various other functional forms for the IMF

[1] For the introduction part of this thesis, we're using the format of the introduction part of the Bastian et al. [2010] review on IMF due to its exclusiveness and summarize some of the most important and related topics of it.

has been suggested. Kroupa et al. [1993] suggested a multi-segmented power-law IMF with a shallower slope than the Salpeter's original results at lower masses.

We can also define the IMF in the context of linear mass units

$$\chi(m) = dN/dm \propto m^{-\alpha} \tag{1.2}$$

which enables us to estimate the number of stars within some mass range. Notice that

$$\chi(m) = 1/(m \ln 10)\Phi(\log m) \tag{1.3}$$

yielding the relation

$$\alpha = \Gamma + 1 \tag{1.4}$$

In this study, we're adopting the logarithmic notation but the results can easily be converted to the linear mass notation by using the relation between α and Γ provided above. Having these two different notations has led to enormous confusion in the literature.

Another proposed form for the IMF is the log-normal form. Using the logarithmic notation of the power-law IMF makes it easier to describe the IMF as a log-normal distribution. Miller and Scalo [1979] first introduced the log-normal form of the IMF, but a theoretical explanation was not offered till 1984. Zinnecker [1984] used the central limit theorem to provide a theoretical explanation for the log-normal distribution of the stellar masses. Based on the central limit theorem, any function resulting from the sum of an infinite number of independent variables can be described by a normal or gaussian distribution function (also see Larson [1973]). If we assume that the star formation process is a complex transformation and that the stellar masses are the product of several independent variable, then we can say that $\log m$ has a gaussian distribution (Bastian et al. [2010]). The log-normal form of the IMF (see Adams and Fatuzzo [1996]) has the form

$$\phi(m) \sim e^{-\frac{(\log m - \log m_c)^2}{2\sigma^2}} \tag{1.5}$$

where m_c is called the Characteristic Mass (the stellar mass with the highest frequency) and σ is the dispersion of the log-normal distribution.

In 2005, de Marchi et al. [2005] introduced the "tapered power-law" IMF which has the form

$$\chi(m) = \frac{dN}{dm} \propto m^{-\alpha}[1 - e^{(-m/m_p)^\beta}] \tag{1.6}$$

Where m_p, gives the peak mass, α is the index of the power-law in the upper end of the mass function and β is the "tapering" exponent to describe the lower end of the IMF.

1.2 Observational and Statistical Challenges

A robust empirical measurement of the IMF is a challenge with many uncertainties associated with. In this part of the introduction, we briefly discuss some of the observational and statistical challenges that observational astronomers face when trying to measure the IMF in a stellar population (see Scalo [1986] for an introduction to the IMF construction methodology).

1.2.1 Observational Challenges

There are many difficulties in the observational constraining of the stellar IMF. Here, we'll discuss three of the most important issues which affect almost every IMF studies. The first challenge is that we need to have stellar populations with enough numbers of low-mass and high-mass stars so that we can effectively constrain our IMF parameters. In order to choose samples like this, we'll need to choose large stellar populations for our studies which is not always possible. Most of the IMF studies are trying to detect variations in the IMF. Measuring the IMF of the Milky Way disk which is a very complex and multi-component stellar population provides a very useful case study. First step seems trivial: counting the stars in our sample and measuring their masses. Trying

to choose large samples in a system like this results in having stars from different populations and star formation events. One should assume that the IMF is constant over a large volume. The other issue that we're dealing with in this case is that stars' lifetimes are finite. There's a high chance that a fraction of the high-mass stars in the regions that we study are well evolved of the main sequence and are not present in our sample anymore. So we can only measure the Present Day Mass Function of Stars (PDMF) in our samples with some fractions of the high-mass stars missing. Every star with $M \leq 0.8 M_{\odot}$ that was ever formed is still present in the Galactic disk, however, and thus will be represented in the PDMF. Determining the IMF from the PDMF requires the assumption that the IMF does not vary with time! Moreover, we'll need a thorough knowledge of the Star Formation History (SFH) of the Galaxy. Even if we have these knowledge, there are still degeneracies involved in inferring the IMF from the PDMF (Elmegreen and Scalo [2006]). Deviations from the Salpeter IMF are mainly seen on the low-mass end of the IMF which is where corrections need to be made (around one solar mass). The last observational issue that we will discuss here is the multiplicity of stellar objects. Most of the stellar systems are found to have gravitationally bound companions of lower masses at a variety of orbital configurations. It's not always easy to detect these companions and in most cases it actually is impossible to count for the companions directly. These unresolved systems can result in a significance uncertainty in the IMF constraints if we assume that most of the IMF studies use monochromatic luminosity functions (Kroupa [2001]; Chabrier [2003]; Maíz Apellániz [2008]). Correcting for this issue is not a straightforward task as it both depends on the binary fraction and the mass ratio of the stellar systems involved. Observational studies reveal that multiplicity declines with primary mass (e.g. Lada [2006]): the initial binary frequency of O stars may be as high as 100% (Mason et al. [2009]) dropping to $\sim$ 60% for solar-type stars (Duquennoy and Mayor [1991]), $\sim$ 30% for early M stars (Fischer and Marcy [1992]), and to 20% or less for very-low mass objects (M<0.1 $M_{\odot}$; Bouy et al. [2003]). On the other hand, the mass ratio is also mass dependent. with typical O star mass ratios near unity (Zinnecker and Yorke [2007]), a flat distribution of (detectable) mass ratios between 0.1 and 1.0 for solar type stars, and a preference towards equal mass systems for the lowest mass binaries.

1.2.2 Statistical Considerations

As we mentioned earlier, there are many different sources of uncertainties in the IMF studies which could result in significant measurement errors. In most of the IMF studies, astronomers fit either power-law or log-normal IMF forms to their data and then they compare their results to other IMF studies. Making such comparisons can get very tricky because of the many sources of uncertainty and assumptions made in the IMF studies. A disagreement between the derived parameters is typically interpreted as indicative of astrophysically meaningful IMF variations (Bastian et al. [2010]). Also, some studies do not provide uncertainties associated with their measurements which makes these comparisons even more difficult to make. It's obvious that using more complicated functional forms for the IMF (with more free parameters) would result in better fits but one should make sure that differences between two IMF fitting results is statistically significant. Otherwise, we're tracking down variations which are not statistically significant. Statistical tests such as the F-test can help with choosing an appropriate functional form for the IMF in different studies. Another important point that one should be aware of is that the IMF analyses are highly mass-range dependent. Two different IMF analyses can indicate different constraints on the parameters or even different analytic forms if they are done for different mass ranges (even if from the same parent population). How the data were binned can also be a source of difference between different studies. Statistical tests such as the Kolmogorov-Smirnov (KS) test can help us to compare different studies regardless of how the binning were done but we shouldn't forget that the results of these tests are sensitive to systematic differences.

Studies of the local field, local young clusters and old globular clusters suggest that most of them were drawn from a universal IMF: a power-law of Salpeter index (Γ = 1.35) above a few solar masses, and a log-normal or shallower power-law ($\Gamma \sim 0$ - 0.25) between a few tenths and a few solar masses. Chabrier (2003, 2005) parameterized the IMF below 1 $M_\odot$ as a log-normal distribution with a characteristic mass $m_c \sim 0.22 M_\odot$ for the system mass function and $m_c \sim 0.08 M_\odot$ for the single objects mass function. Most of the uncertainty lies in the regime of solar-subsolar regime, and the question of universality or locality of IMF is still under investigation (for instance, see Geha

et al. [2013] and Kalirai et al. [2013]). Some astronomers believe that the low-mass IMF should depend on the physical properties of the star formation event such as the gas density, metallicity, or turbulent velocity (e.g.,Larson [2005]; Bate [2009]; Myers et al. [2011]), however, IMF measurements are largely invariant within the Milky Way (Covey et al. [2008]). Recent indirect studies suggest that the low-mass IMF slope does vary outside the Milky Way (Treu et al. 2010; van Dokkum & Conroy 2011; Cappellari et al. 2012a; Dutton et al. 2012; Conroy & van Dokkum 2012).

Dwarf galaxies have very low metallicities (~ -2.0) and have relaxation times longer than a Hubble time. Therefore, there's no need to make dynamical evolution corrections for them. Dwarf galaxies in which the low mass IMF has been directly measured are the Ursa Minor ([Fe/H] = -2.0), Draco ([Fe/H] = -2.0), and the Small Magellanic Cloud (SMC; [Fe/H] = -1.2). Wyse et al. (2002) found that the Ursa Minor IMF is consistent with a power-law slope $\Gamma = 0.8$ over the mass range 0.4 - 0.7 $M_{\odot}$. Grillmair et al. (1998) constrained a power-law slope for the Draco dwarf galaxy between $1.1 < \Gamma < 1.3$ for an assumed age of 12 Gyr, based on HST/WFPC2 imaging extending to 0.6 $M_{\odot}$. Kalirai et al. (2013) used HST/ACS data to conclude that the IMF of the SMC has a power-law slope of $\Gamma = 0.90^{+0.10}_{-0.15}$ over the mass range 0.37 - 0.93 $M_{\odot}$. Moreover, Geha et al. (2013) studied two ultra-faint dwarf (UFD) galaxies: Hercules and Leo IV. For Hercules, they constrained a power-law IMF with a slope of $\Gamma = 0.2^{+0.4}_{-0.5}$ over a mass range of 0.52 - 0.76 $M_{\odot}$. For Leo IV, they found a single-sloped power-law IMF slope of $\Gamma = 0.3 \pm 0.8$ over a mass range of 0.54 - 0.77$M_{\odot}$. While, for a log-normal IMF with a fixed dispersion of 0.69, they found a characteristic mass of $0.4^{+0.9}_{-0.3}M_{\odot}$ for Hercules and a characteristic mass of $0.4^{+2.1}_{-0.3}M_{\odot}$ over the same mass ranges as for their power-law analyses.

The Draco dwarf spheroidal (dSph) galaxy is among the faintest and lowest surface brightness known members of the Local Group of galaxies [Mateo, 1998]. It appears to be dominated by very old (age greater than 8 - 10 Gyr) and metal deficient stellar populations Aparicio et al. [2001]. Moreover, it is reported to have the highest M/L ratio (e.g. up to M/L = 300 - 1000: see Kleyna et al. [2001]) (see Table 2.1). All these exceptional properties make the Draco a unique study case. The thesis is organized in the following way: in §2, we talk about the observations and data sampling. In §3, we

talk about the IMF analyses and results, while in §4 we summarize the main points.

Chapter 2

Observations and data analysis

In this study, we have used archival data from Hubble Space Telescope (HST) Advanced Camera for Surveys (ACS) and Wide Field Camera 3 (WFC3) under program number GO-12966 which was initially proposed to address the core-cusp problem (Figure 2.1). Observations include 3 fields in the Draco dwarf Spheroidal (dSph) at 3 different radii to the center of the galaxy. Field number one is at a distance of approximately 255pc from the center while fields number two and three are ∼315 and ∼145pc away from the center, respectively. We performed Point-Spread Function (PSF) photometry using the DOLPHOT photometry package Dolphin [2000] and ran ∼100k artificial star tests per field to quantify the completeness and photometric uncertainties.

2.1 Data Sampling For The Power-Law IMF

After doing the photometry and in order to choose an appropriate sample for analysis, magnitude limits for different fields with a 50% completeness on the faint ends are set as the following. For field number 1, bright limits are 23.3 and 22.9 and faint limits are 27.1 and 26.0 for UVIS606W and UVIS814W filters, respectively. For field number 2, bright limits are 23.3 and 22.9 and faint limits are 27.1 and 26.0 in WFC606W and WFC814W filters, respectively. For field number 3, bright limits are 23.5 and 23.0, while faint limits are 27.3 and 25.9 in WFC555W and WFC814W filters, respectively. These regions are identified as green regions on the CMDs in Figure 2.2. These limits

Table 2.1 **Draco dSph Galaxy Properties**

Quantity	**Units**	**Value**
$\alpha(J2000)$	$h:m:s$	$17:20:12$
$\delta(J2000)$	$^\circ:\prime:\prime\prime$	$+57:54:55$
l	$^\circ$	86.4
b	$^\circ$	34.7
$(m-M)_V$[a]	mag	19.54
$Distance$[b]	kpc	82 ± 6
$E(B-V)$[a]	mag	0.07
$log(M_\star/M_\odot)$[c]		5.43 ± 0.10
$log(L_V/L_\odot)$[c]		5.51 ± 0.10
M_V[f]	mag	-9.0 ± 0.3
M_{total}[d]	$M_\odot$	3.90×10^8
$\langle[Fe/H]\rangle$[c]	dex	-1.98 ± 0.01
V_{los}[e]	km/s	291.0 ± 0.1
r_{half}[b]	pc	196 ± 12

[a] Distance modulus and extinction from Weisz et al. [2014].
[b] Distance and projected half-light radius as listed by Nayakshin and Wilkinson [2013].
[c] Stellar mass, observed V-band luminosity and metallicity as listed by Kirby et al. [2013] and references therein.
[d] Total mass from Sohn et al. [2013].
[e] Line of sight velocity from Pawlowski and Kroupa [2013].
[f] V-band absolute magnitude from Bellazzini et al. [2002].

sample a mass range of 0.5 - $0.8M_\odot$.

2.2 Data Sampling For The Log-Normal IMF

Like the power-law data sampling, in order to choose an appropriate sample for analysis, magnitude limits for different fields are set as the following. First of all, for all of the fields we choose a 50% completeness on the faint end. For field number 1, bright limits are 23.3 and 22.9 and faint limits are 28.3 and 26.5 for UVIS606W and UVIS814W filters, respectively. For field number 2, bright limits are 23.3 and 22.9 and faint limits are 28.1 and 26 in WFC606W and WFC814W filters, respectively. For field number 3, bright limits are 23.5 and 23.0, while faint limits are 27.3 and 25.9 in WFC555W and WFC814W filters, respectively. Green regions on the CMDs in Figure 2.3 are the

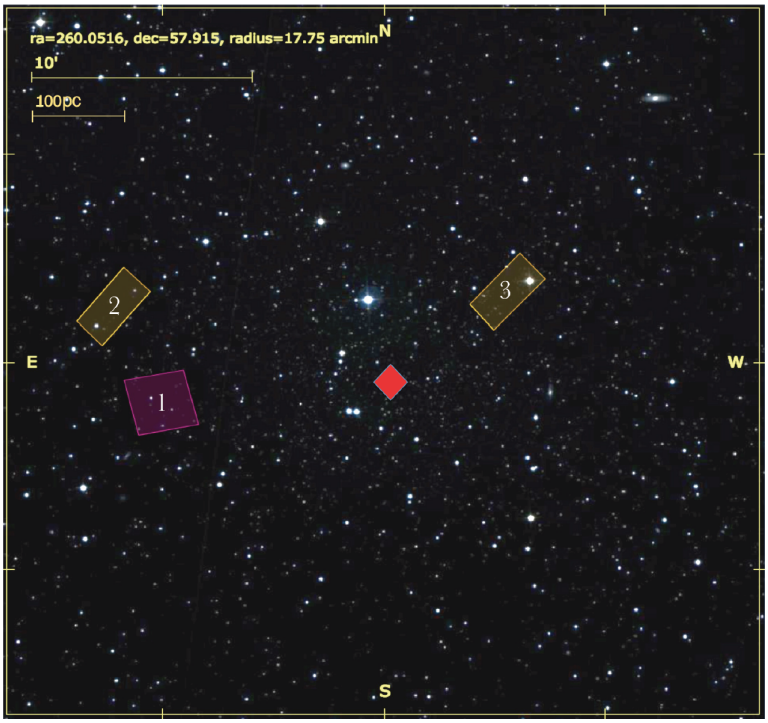

Figure 2.1 Position of observed fields in the Draco galaxy on the sky. Observations for field number 1 is done by WFC3/UVIS while data for fields number 2 and 3 are taken by ACS/WFC. Angular scale shown on the image corresponds to a physical distance of ∼0.24 kpc. The red diamond symbol shows approximately the center of the Draco galaxy.

corresponding populations. These limits correspond to a mass range of $0.5 - 0.8 M_{\odot}$. We have pushed our faint end limits to higher magnitudes in order to include more stars in our CMDs. This is crucial for log-normal IMF analysis as we need to have more data to constrain a more complicated functional form in this case. Moreover, by pushing the faint limits to higher magnitudes, we cover a slightly larger mass range which in turn results in better constraints on our log-normal IMF parameters. We note that these deeper CMDs cover a mass range slightly larger than our power-law samples. These differences are smaller than our analysis accuracy levels. So we report the results for the log-normal IMF for the same mass range as of the power-law IMF.

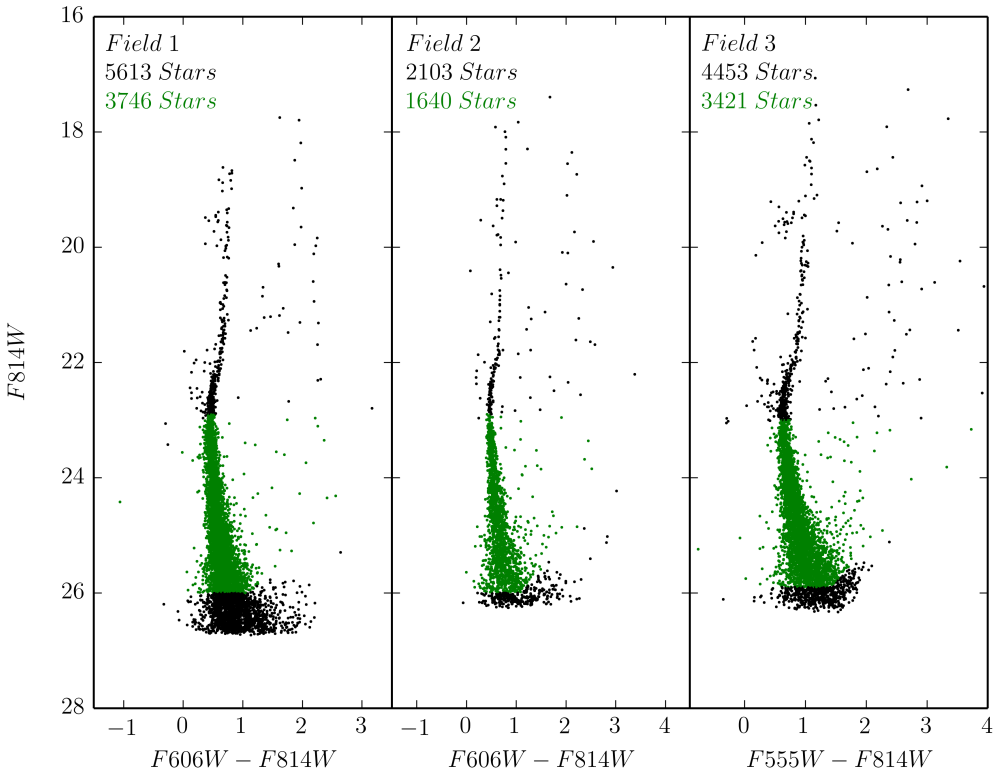

Figure 2.2 The HST /ACS and WFC3 CMDs for the three fields in Draco galaxy studied. Green regions are corresponding to a mass range of 0.5-0.8 $M_{\odot}$ and have been chosen for our power-law IMF analysis. The total number of stars and the number of stars in each sampled CMD is denoted on the CMDs with black and green colors respectively.

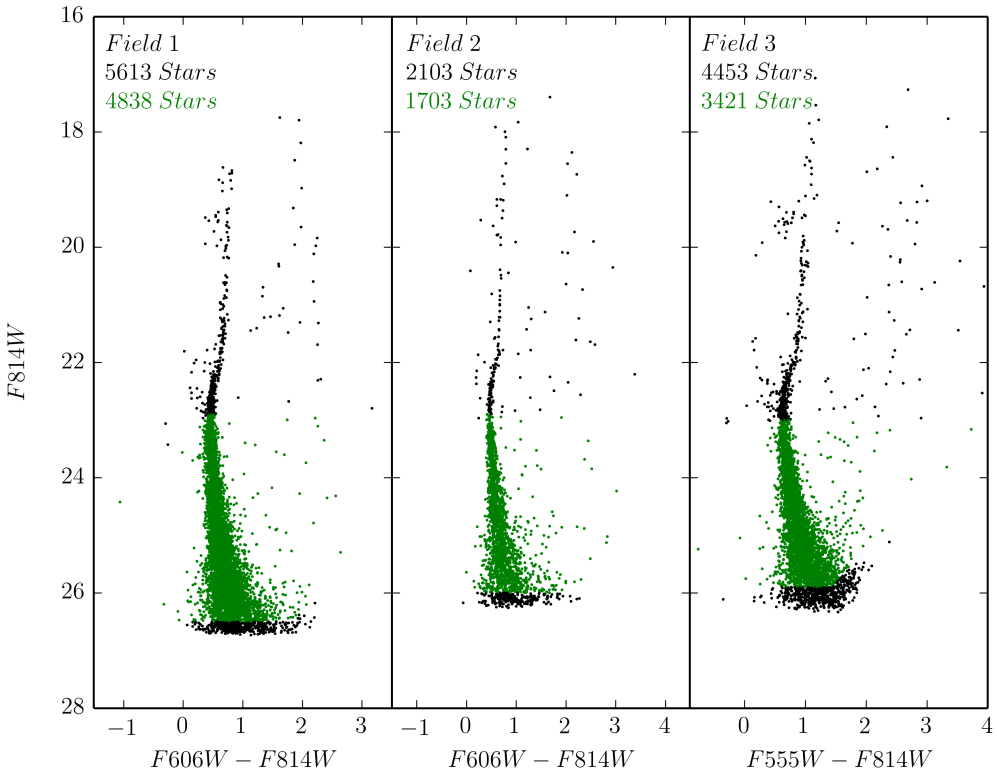

Figure 2.3 The HST /ACS and WFC3 CMDs for the three fields in Draco galaxy studied. Green regions are corresponding to a mass range of ∼0.5-0.8 $M_{\odot}$ and have been chosen for our log-normal IMF analysis. The total number of stars and the number of stars in each sampled CMD is denoted on the CMDs with black and green colors respectively.

Chapter 3

IMF Analysis And Results

We fit two different IMF models (power-law and log-normal) to our data using the CMD fitting program MATCH Dolphin [2002]. MATCH constructs synthetic CMDs of stellar populations from user-defined parameters including a stellar IMF, binary fraction, a searchable range of distance and extinction values, fixed values of age, metallicity and bins in color and magnitude. It then convolves the model CMD with observational biases as measured from the artificial star tests. MATCH computes the likelihood of the data given the model CMD using a Poisson likelihood statistic, enabling the characterization of the physical properties of a resolved stellar population.We have utilized Dartmouth, BaSTI, Padova, Victoria and PARSEC stellar evolutionary tracks and models (Dotter et al. [2008]; Marigo et al. [2008]; Girardi et al. [2010]; Pietrinferni et al. [2004]; VandenBerg et al. [2006]; Bressan et al. [2012]) in our studies. The use of multiple stellar models is particularly important for CMD analysis, as the systematic differences between stellar evolution libraries are frequently the dominant source of uncertainty in stellar population analysis. In §3.1 we will talk about the Power-law IMF analysis and in §3.2 we are presenting the Log-normal IMF fitting procedure and results.

3.1 Power-Law IMF Analysis

We analyzed the regions as follows. We first adopt a distance modulus $(m-M)_V = 19.50$ and extinction $A_V = 0.07$ Weisz et al. [2014]. Then, we run MATCH for different combinations of IMF slope (Γ) and Binary Fraction. As mentioned before, MATCH

then uses a Poisson likelihood statistics to return a value indicating the goodness of the fits. For the IMF fits, we set up a grid with resolution of 0.1 in Binary Fraction (BF) and 0.2 in IMF slope (Γ). Our complete set of fits surveys the full space in BF (0 to 1) and a range of IMF slopes between 0.35 and 2.35 in order to investigate both shallower and steeper IMFs compared to Salpeter's IMF ($\Gamma = 1.35$). Having goodness measures of the fits in hand, we have constructed confidence contours and plotted them up to 3σ error levels. Moreover, a cubic spline interpolation routine has been implemented to get smoother contours(Figure 3.1). Our analysis reveals that using different stellar models can result in drastic changes in both IMF slope (Γ) and Binary Fraction values (Table 3.1 and Figure 3.1). Moreover, analysis results indicate inconsistencies between IMF slope and Binary Fraction for different fields, at least, at the 1σ significance as can be seen from the confidence contours (Figure 3.1). For the BaSTI stellar model, we can see that there is a significant difference in IMF slope and Binary Fraction values between field number 3 and the other two fields while the two other fields agree on the same IMF slope and BF at a 1σ significance level. For the Dartmouth model, we can see that BF values are somewhat consistent for all the fields while the IMF slopes are different up to a 2σ confidence level for different fields. For the Padova model, we can see that Binary Fraction is again consistent for all of the fields to a good extent while the IMF slopes are varying from field to field. In the next step and in order to check the goodness of our fits, simulated Luminosity Functions (LFs) have been constructed using the FAKE module in MATCH for the best fit values, $+1\sigma$ fit values and -1σ fit values of our constrained IMF parameters. Results can be seen in figures 3.1.

Regardless of the stellar model chosen, we have detected a radial dependence of the power-law IMF's slope (Γ). Depending on the stellar model choice, up to $\sim$0.7 dex increase in Γ can be seen when galactocentric distance is increasing from 145pc to 315pc (see Fig. 3.3). We rule out the mass segregation scenario for this observation because of the very small size of the galaxy compared to its huge dark matter halo. Also, as mentioned earlier, dwarf galaxies have extremely long relaxation times so there's no need to correct for dynamical evolution. It can also be seen that the value of the Binary Fraction (BF) is tightly tied to the stellar model utilized. BaSTI models always predict the largest binary fraction and Dartmouth models always detect the smallest binary fraction (see Fig. 3.3). We don't see any radial dependencies in the binary fraction

Table 3.1 **Draco dSph Galaxy Power-Law IMF Results**

Field	Stellar Model[a]	Γ	**Binary Fraction**
	BaSTI	1.29 ± 0.16	0.76 ± 0.05
	Dartmouth	1.56 ± 0.15	0.27 ± 0.03
Field 1	Padova	0.89 ± 0.15	0.48 ± 0.04
	Victoria	1.38 ± 0.17	0.58 ± 0.04
	PARSEC	1.16 ± 0.15	0.45 ± 0.04
	BaSTI	1.79 ± 0.24	$> 0.86 \pm 0.12$
	Dartmouth	1.83 ± 0.22	0.38 ± 0.07
Field 2	Padova	1.16 ± 0.22	0.49 ± 0.08
	Victoria	1.68 ± 0.28	0.71 ± 0.08
	PARSEC	1.38 ± 0.27	0.63 ± 0.11
	BaSTI	1.27 ± 0.18	0.82 ± 0.11
	Dartmouth	1.16 ± 0.17	0.37 ± 0.05
Field 3	Padova	0.65 ± 0.16	0.47 ± 0.07
	Victoria	1.06 ± 0.19	0.66 ± 0.06
	PARSEC	0.83 ± 0.17	0.59 ± 0.05

[a] References for stellar evolutionary models and isochrones are Dotter et al. [2008]; Marigo et al. [2008]; Girardi et al. [2010]; Pietrinferni et al. [2004]; VandenBerg et al. [2006]; Bressan et al. [2012].

values. We believe that the tight dependency of the BF on the stellar model is because of the slight slope difference of the main sequence of different stellar libraries.

Dartmouth stellar evolutionary tracks are made for 4 different values of Alpha element enhancement (α): -0.2, 0.0 (solar), 0.2, 0.4. We have fitted power-law IMFs to our data using all of these different possibilities. As it can be seen in Fig 3.4, using models with different values of α, does not change the slope of the IMF or the fitted BF value significantly. This can either be because of the fact that we have broadband images or that there's no α dependence in the IMF slope and BF characteristics.

3.2 Log-Normal IMF Analysis

Similar to the power-law IMF analysis, we first adopt a distance modulus $(m - M)_V = 19.50$ and extinction $A_V = 0.07$ Weisz et al. [2014]. Then, we run MATCH with a log-normal IMF over our data in order to constrain the Binary Fraction and Characteristic values of a log-normal IMF: Characteristic Mass (m_c) and Dispersion (σ). Here, as

mentioned earlier, we fit for CMD regions which go slightly deeper than the regions used in the power-law analysis (see fig. 2.3). Running MATCH with these three free parameters shows a significant degeneracy in the $\sigma - m_c$ plane which can indicate that our data is not deep enough to need a log-normal IMF to describe it. Hence, we conclude that a power-law IMF describes the data that we have in hand pretty well and there's no need to introduce a log normal IMF in this region of the CMDs. In the next section of the paper, we'll do some simulation studies to show how the deepness of the data can affect the degeneracy in the $\sigma - m_c$ plane. In this section of the paper, we adopt two different fixed values for σ and try to constrain the Characteristic Mass (m_c) and the Binary Fraction. Chabrier [2003] reports two different values for σ of the Galactic mass function (MF) below $1M_{\odot}$: $\sigma = 0.69$ for single objects and $\sigma = 0.57$ for the system MF. We've fitted log-normal IMFs with fixed values of σ to these two values and have presented the confidence contours for the $m_c - BF$ plane (Figures 3.6 and 3.7). Moreover, quantitative results can be found in tables 3.2 and 3.3.

Table 3.2 **Draco dSph Galaxy Log-Normal IMF Results ($\sigma = 0.57$)**

Field	Stellar Model[a]	m_c	**Binary Fraction**
	BaSTI	0.02 ± 0.01	0.28 ± 0.04
	Dartmouth	0.06 ± 0.01	0.26 ± 0.02
Field 1	Padova	0.28 ± 0.05	0.50 ± 0.04
	Victoria	0.10 ± 0.02	0.63 ± 0.05
	PARSEC	0.11 ± 0.02	0.44 ± 0.03
	BaSTI	0.03 ± 0.01	0.82 ± 0.12
	Dartmouth	0.03 ± 0.01	0.38 ± 0.08
Field 2	Padova	0.08 ± 0.02	0.51 ± 0.08
	Victoria	0.03 ± 0.02	0.74 ± 0.07
	PARSEC	0.06 ± 0.03	0.71 ± 0.08
	BaSTI	0.08 ± 0.02	0.86 ± 0.09
	Dartmouth	0.09 ± 0.03	0.38 ± 0.04
Field 3	Padova	0.22 ± 0.06	0.53 ± 0.04
	Victoria	0.10 ± 0.03	0.70 ± 0.04
	PARSEC	0.15 ± 0.05	0.58 ± 0.03

[a] References for stellar evolutionary models and isochrones are Dotter et al. [2008]; Marigo et al. [2008]; Girardi et al. [2010]; Pietrinferni et al. [2004]; VandenBerg et al. [2006]; Bressan et al. [2012].

By comparing the constrained Binary Fraction values for these two log-normal IMFs to those of the power-law form, we can see that the BF values agree to a good extent. This shows that the BF can be constrained pretty well regardless of the IMF characteristics. Based on this conclusion, one can try to fit log-normal IMFs with fixed values of BF to the existing data, but the degeneracy in the $\sigma - m_c$ plane won't still go away.

Table 3.3 **Draco dSph Galaxy Log-Normal IMF Results ($\sigma = 0.69$)**

Field	Stellar Model[a]	m_c	**Binary Fraction**
	BaSTI	0.02 ± 0.01	0.21 ± 0.03
	Dartmouth	0.02 ± 0.01	0.26 ± 0.02
Field 1	Padova	0.20 ± 0.05	0.50 ± 0.04
	Victoria	0.05 ± 0.01	0.62 ± 0.05
	PARSEC	0.06 ± 0.02	0.44 ± 0.03
	BaSTI	0.02 ± 0.01	0.80 ± 0.13
	Dartmouth	0.02 ± 0.01	0.42 ± 0.07
Field 2	Padova	0.04 ± 0.02	0.52 ± 0.08
	Victoria	0.03 ± 0.01	0.77 ± 0.07
	PARSEC	0.03 ± 0.02	0.72 ± 0.07
	BaSTI	0.03 ± 0.02	0.87 ± 0.09
	Dartmouth	0.03 ± 0.02	0.38 ± 0.05
Field 3	Padova	0.13 ± 0.06	0.53 ± 0.04
	Victoria	0.05 ± 0.02	0.70 ± 0.03
	PARSEC	0.02 ± 0.01	0.74 ± 0.06

[a] References for stellar evolutionary models and isochrones are Dotter et al. [2008]; Marigo et al. [2008]; Girardi et al. [2010]; Pietrinferni et al. [2004]; VandenBerg et al. [2006]; Bressan et al. [2012].

Our results for a fixed-dispersion log-normal IMF shows that, for the BaSTI, Dartmouth and Victoria models, characteristic masses for our three fields are in good agreement while for the Padova model we can see some variations in the characteristic mass. On the other hand, for the Dartmouth, Padova and Victoria models, we can see a good agreement between the constrained BF values while for the BaSTI model, the BF for field number 1 is constrained to a much lower value compared to the other two fields. Moreover, we can see that for almost all of the models and fields we get a larger value for the characteristic mass when we have a smaller values for the dispersion. We would like to point out that the shift in characteristic mass seen in our results is much smaller

than the shift seen for the Galactic MF Chabrier [2003]. The later result shouldn't be surprising as it follows from the behavior of a log-normal distribution.

3.3 Simulation Studies of The IMF

Simulation studies have been used previously to demonstrate the strength of MATCH in simulating CMDs and recovering input parameters. For instance, in Dolphin [2002] a few different synthetic CMDs with different Star Formation Histories (SFHs) have been generated using the FAKE module in MATCH. This module creates synthetic CMDs given a predefined set of parameters such as a stellar library, IMF, SFR and metallicities at different age bins. In Dolphin [2002], synthetic single and composite stellar populations have been generated and then MATCH is run over them to see how the FAKE input parameters can be recovered from simulations. Simulation results indicate that the recovered parameters are in great agreement with the FAKE input parameters (SFR and Z in this case). In this thesis, we try to do some simulation studies to show how powerful and reliable MATCH is in recovering IMF parameters. We have created synthetic CMDs with different IMF characteristics, different number of stars and different theoretical stellar evolutionary tracks and isochrones and then have tried to recover those characteristics using MATCH. All of our synthetic CMDs have a single stellar population (SSP) with an age of $\sim 10\ Gyr$. Moreover, a metallicity [Fe/H] of -1.5 has been adopted in all of our synthetic CMD generations. Furthermore, we're generating fake stars for our models in WFC606W and WFC814W filters. We populate our sythetic CMDs with stars with magnitudes between -5 and 20 for the WFC606W and between -4 and 20 for the WFC814W. Different stellar models cover different stellar mass ranges, so not all of the CMDs have the whole magnitude ranges populated. By setting those limits, we make sure that FAKE covers the whole mass range that the stellar model can generate. In the first set of the simulations we're using a SFR of $10^{-1} M_{\odot}/year$ for the BaSTI library while we set a SFR of $10^{-2} M_{\odot}/year$ for all of the other libraries. Our analyses show that the BaSTI stellar model is the most sensitive model among those we used to the number of stars on the CMD (or equally the whole stellar mass of the cluster). This is why we are using an order of magnitude higher SFR for the BaSTI model analyses. We'll provide more details on the dependencies of the

BaSTI library on the CMD's number of stars in the last part of the simulations. The following scenarios have been studied in our simulations:

(i) Matching IMF Types

(a) For every stellar library, a very deep synthetic CMD has been populated using the aforementioned parameters, a power-law IMF with $\Gamma = 1.35$ and a binary fraction of 35%. Then, MATCH was run over the whole synthetic CMD with Γ (assuming a power-law IMF), BF, SFR and Z as free parameters. Confidence intervals for fitted Γ and BF are illustrated in figure 3.8 up to 3σ level. Simulation results show that input parameters have been recovered in a very good way for almost all of the stellar models.

(b) In this part, a deep artificial CMD has been generated using a log-normal IMF with a dispersion of $\sigma = 0.30$ and a characteristic mass of $m_c = 0.45 M_{\odot}$.The binary fraction is again set to be 35%. This time, MATCH is run over the data assuming a log-normal IMF and the resulting confidence intervals are presented in figure 3.8.

By looking at the confidence contours in figure 3.8, we can obviously see that if the underlying IMF (the IMF which generates the CMD) type is the same as the IMF type that we use for fitting our data, then MATCH can recover the IMF input parameters perfectly.

(ii) Non-Matching IMF Types

(a) In this study, we've created an artificial CMD based on a log-normal IMF with a σ of 0.69 and a m_c of $0.08 M_{\odot}$. Then have fitted the whole stellar mass range with a power-law IMF. Again IMF slope (Γ), BF, SFR and Z are our free parameters. Resulting confidence intervals are presented in figure 3.9.

(b) A very similar approach as the previous set of simulations. The only difference is that here, we're using different values for the log-normal IMF than the previous study. Here, dispersion of the distribution is 0.57 and the characteristic mass is $0.22 M_{\odot}$. Confidence contours for this study are presented

in the lower half of figure 3.9.

By comparing the contours in figure 3.9, we find out that different stellar models predict the same values for Γ and BF at least at the 2-σ level. Although the recovered BF is slightly different than the input BF (0.35), all the stellar models predict a similar value for BF. Moreover, by comparing the results for the two different scenarios in this case, we realize that MATCH has reported a shallower power-law IMF when the Characteristic mass is higher (or when the dispersion is smaller).

(c) In the next study, we're creating a fake CMD based on a power-law IMF with a slope of $\Gamma = 1.35$ and a BF of 0.35. Then, we use MATCH to fit a log-normal to our CMD. We're solving only for m_c and σ in this case and fix the BF to 0.35. Results of this study can be found in figure 3.10. As we can see, fitting a log-normal model to a power-law distribution results in getting a Characteristic mass of $\sim$0. This shouldn't be surprising having the definition of m_c in mind. Also, all the stellar models tend to report a very similar Dispersion (σ) of around 0.50.

(iii) Draco-like Simulations

In the next step of our simulation studies, we use the FAKE module in MATCH again to create artificial CMDs more similar to our Draco's observational data. Our fake CMD generation parameters for the previous runs are very similar to the physical properties of Draco. The only change that we need to make is to change the value of SFR to get similar number of stars on the fake CMDs as the observational CMDs. In order to do so, we adopt a SFR of 1.6×10^{-5} for the BaSTI model and a SFR of 1.5×10^{-5} for all of the other models. Another point that we should have in mind is that now we're fitting for a mass range of $0.50 M_{\odot}$ to $0.80 M_{\odot}$. So we should use magnitude limits corresponding to that range and not to fit the whole CMD.

(a) First of all, we make an artificial Draco-like CMD based on a power-law IMF (with $\Gamma = 1.35$) and a BF of 0.35. Then we run MATCH over our CMD

using a power-law IMF in the stellar mass range of 0.50 to 0.80 solar masses. Resulting confidence contours are presented in figure 3.11. We can see that almost all of the stellar models were able to recover the input parameters (Γ and BF) very well. BaSTI tracks predict a slightly higher BF than the input value (0.35). As we mentioned earlier, BaSTI models were always returning the highest BFs in the case of the real data too.

(b) In the next step, we generate artificial CMDs with a log-normal IMF ($\sigma = 0.30$ and $m_c = 0.45 M_\odot$) and then we try to fit a log-normal IMF model to them (see Fig. 3.11). We use an input BF of 0.35 and assume it as known in the runs. So we are just fitting for σ and m_c. As the bottom panel of figure 3.11 shows, our results in the plane of σ-m_c is highly degenerate. We believe that this degeneracy comes only from the low number of the stars and that we're fitting for a mass range which excludes the Characteristic mass value used in generating the fake CMDs.

(c) In the last set of Draco-like simulations, we fit for non-matching underlying IMFs and model IMFs. Confidence contours are present in figure 3.12. In the case of fitting a power-law model to a log-normal underlying distribution, Different stellar model results agree pretty well (at least at a 2σ significance level). While in the case of fitting a log-normal IMF to a power-law distribution, we again struggle with degenerate solutions. The same explanations as the previous step can hold for these solutions too.

(iv) BaSTI Model's Sensitivity to Number of Stars

As we pointed out earlier, BaSTI evolutionary tracks' solutions seem to be the most sensitive ones to the size of the data that we have (or the SFR value). So, in the final set of our simulation studies, we're creating fake CMDs with the BaSTI models and different SFR values. We generate all of the CMDs based on a Salpeter IMF (a power-law with $\Gamma = 1.35$ and BF = 0.35) and use MATCH to fit power-law IMFs to them. We're using SFRs of 10^{-5}, 10^{-4}, 10^{-3}, 10^{-2} and 10^{-1} solar mass/year and fitting results for these different CMDs can be seen in figure 3.13. We're using different units on our axes in figure 3.13 than the previous

figures. Otherwise, the contours are not much larger than the previous solutions. We can see that for almost all of our solutions, confidence contours include the input parameters.

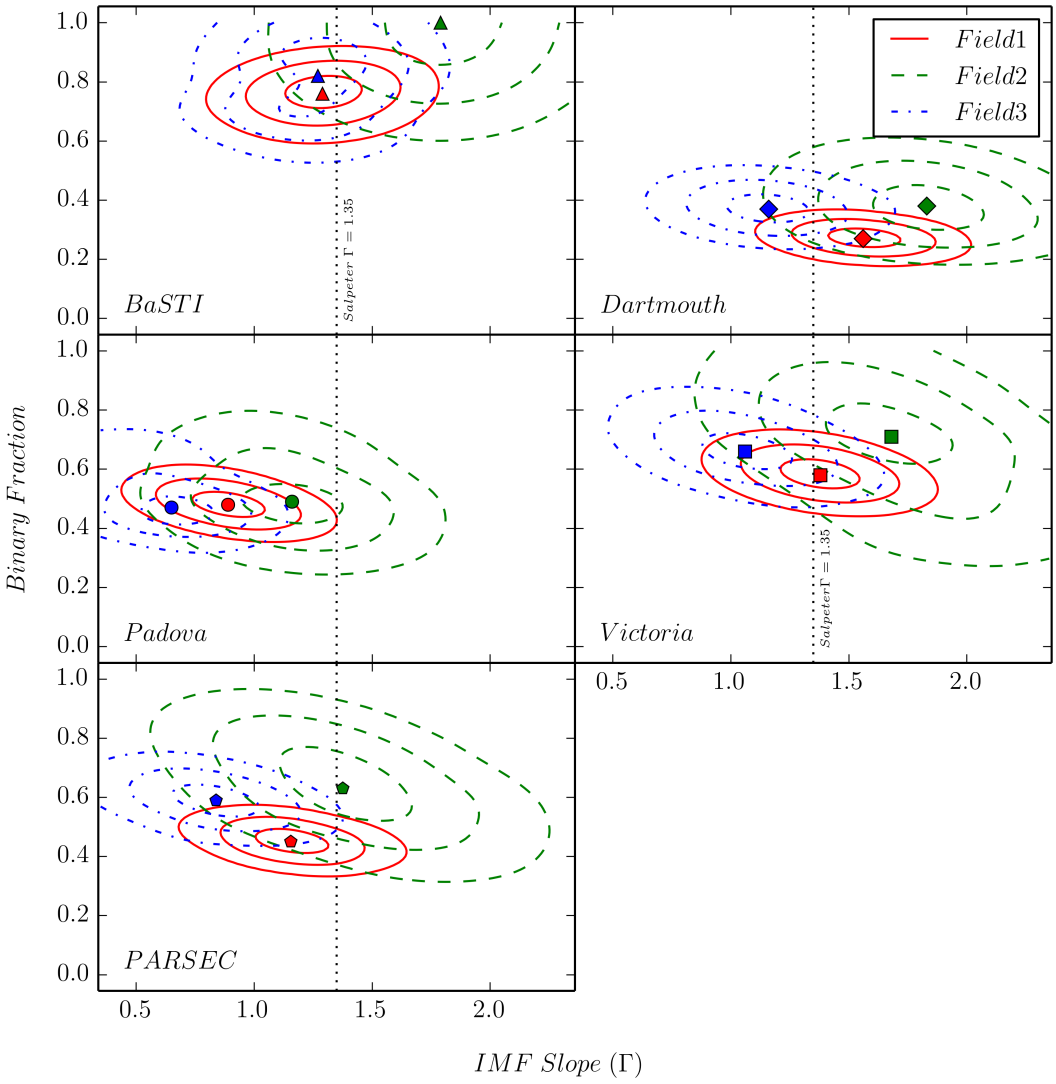

Figure 3.1 Power-law IMF analysis results. Each panel corresponds to one of the stellar models that we have used. In each panel, 3 sets of confidence contours represent the analysis results for different fields studied. Confidence contours are plotted for 1, 2 and 3σ significance levels. Moreover, Salpeter IMF with $\Gamma = 1.35$ is shown for reference.

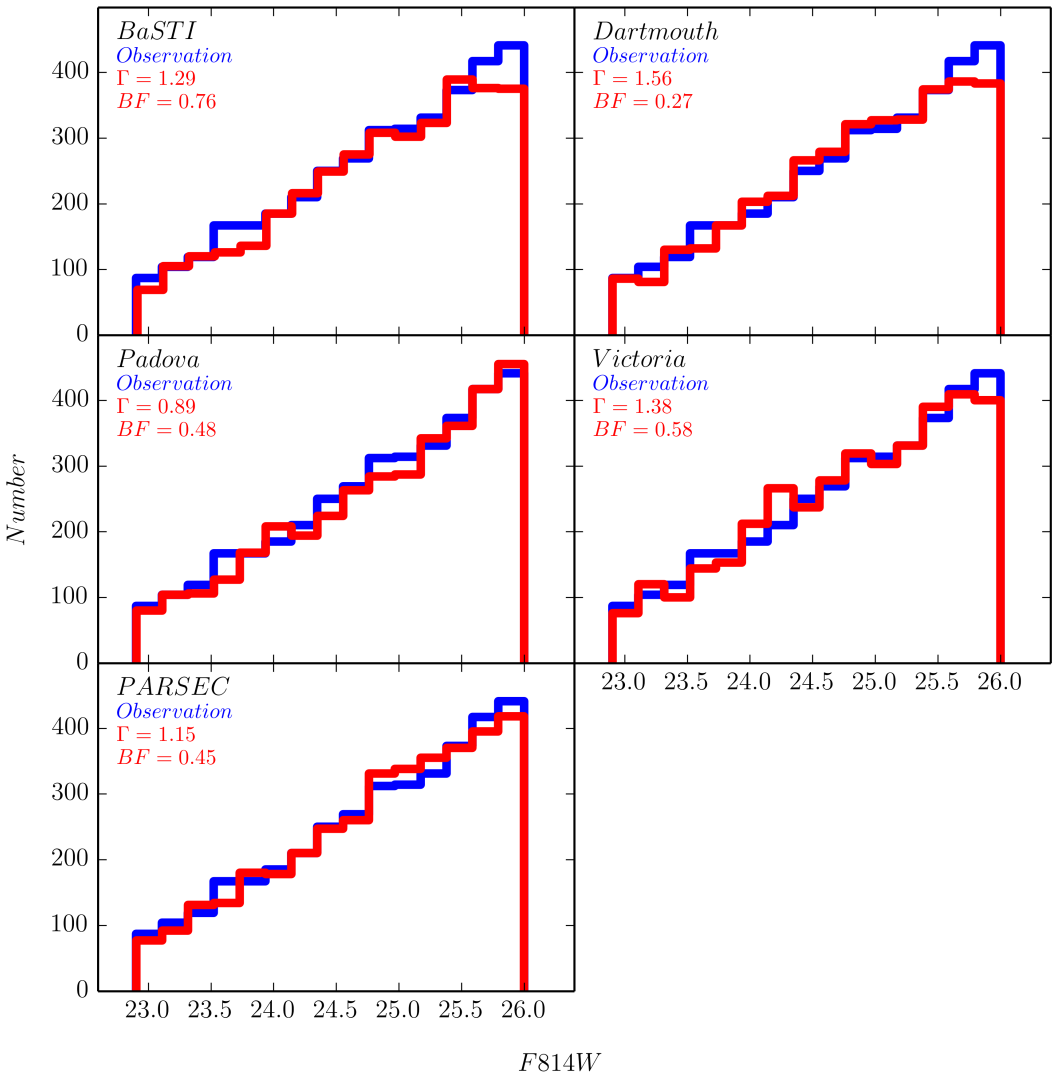

Figure 3.2 Luminosity function comparison plots for field 1. Blue histograms show the data while red histograms are results of CMD simulations with different models using MATCH assuming a power-law IMF. Simulated LFs for other fields match the observational LFs very similar to field 1. So we avoid presenting all the LF plots

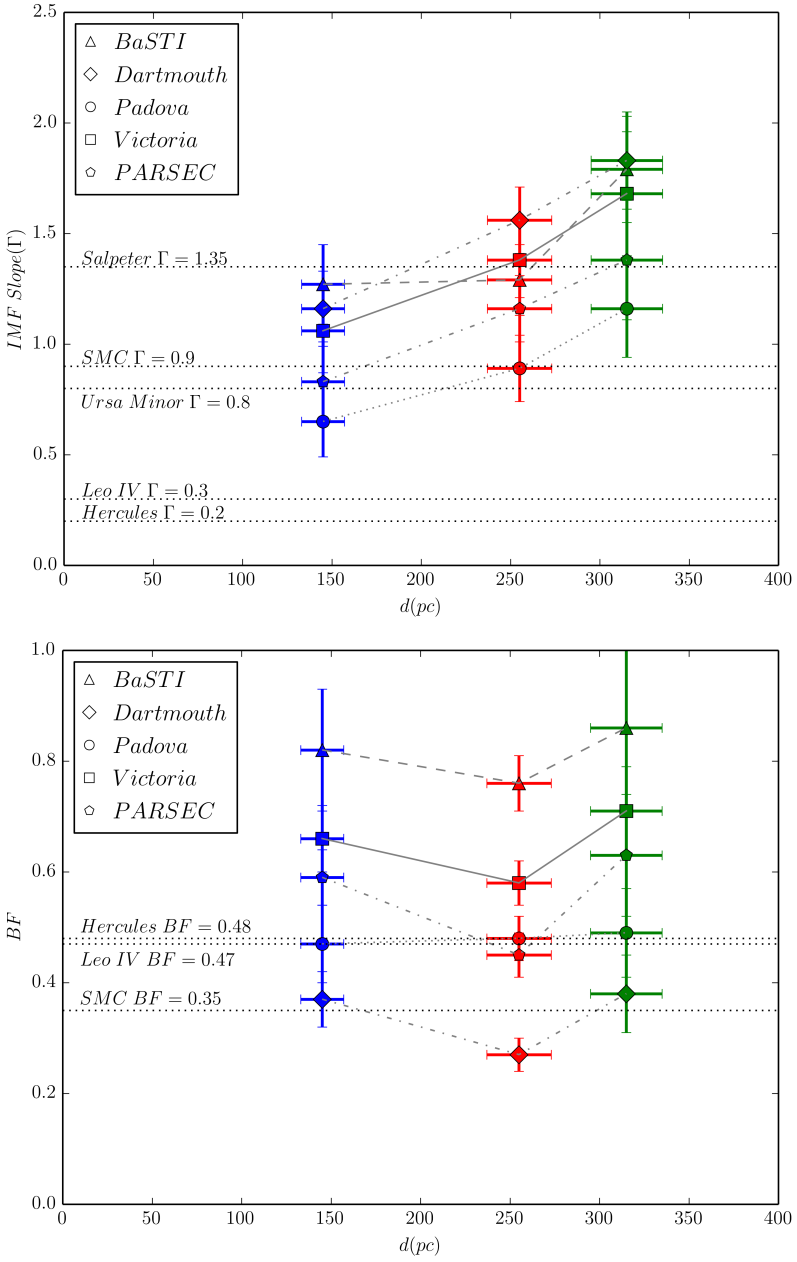

Figure 3.3 Spatial variations of the power-law IMF slope (left) and binary fraction (right). d is the mean galactocentric distance in parsecs. Literature IMF slopes are from Salpeter [1955], Kalirai et al. [2013] and Geha et al. [2013].

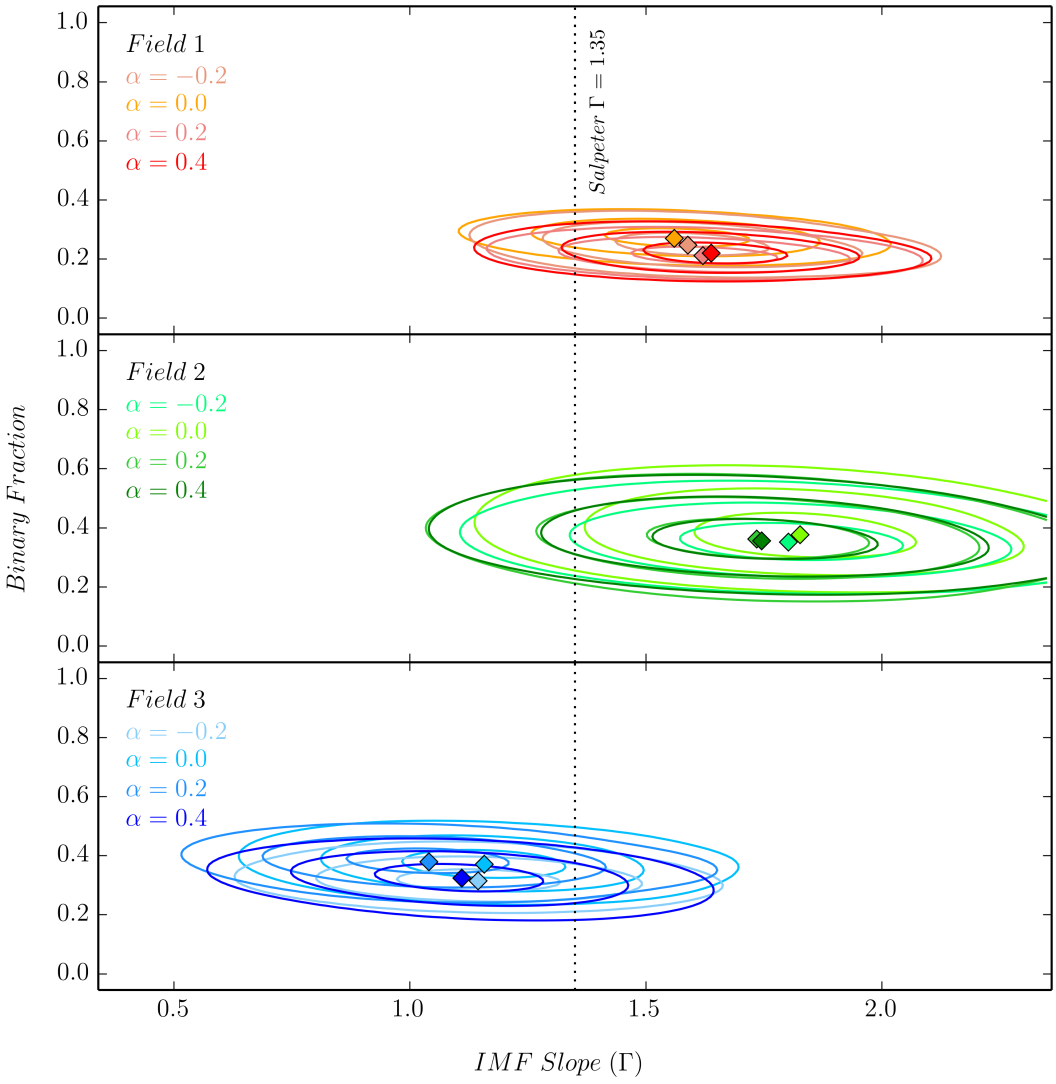

Figure 3.4 Power-law IMF fitting results for the Dartmouth stellar library with different values for Alpha element enhancement ($\alpha = -0.2$, Solar, 0.2, 0.4). Recovered BF and Γ seem to be insensitive to α. This can either be because of the fact that we have broadband observations or that there's no α dependence in the IMF and BF characteristics.

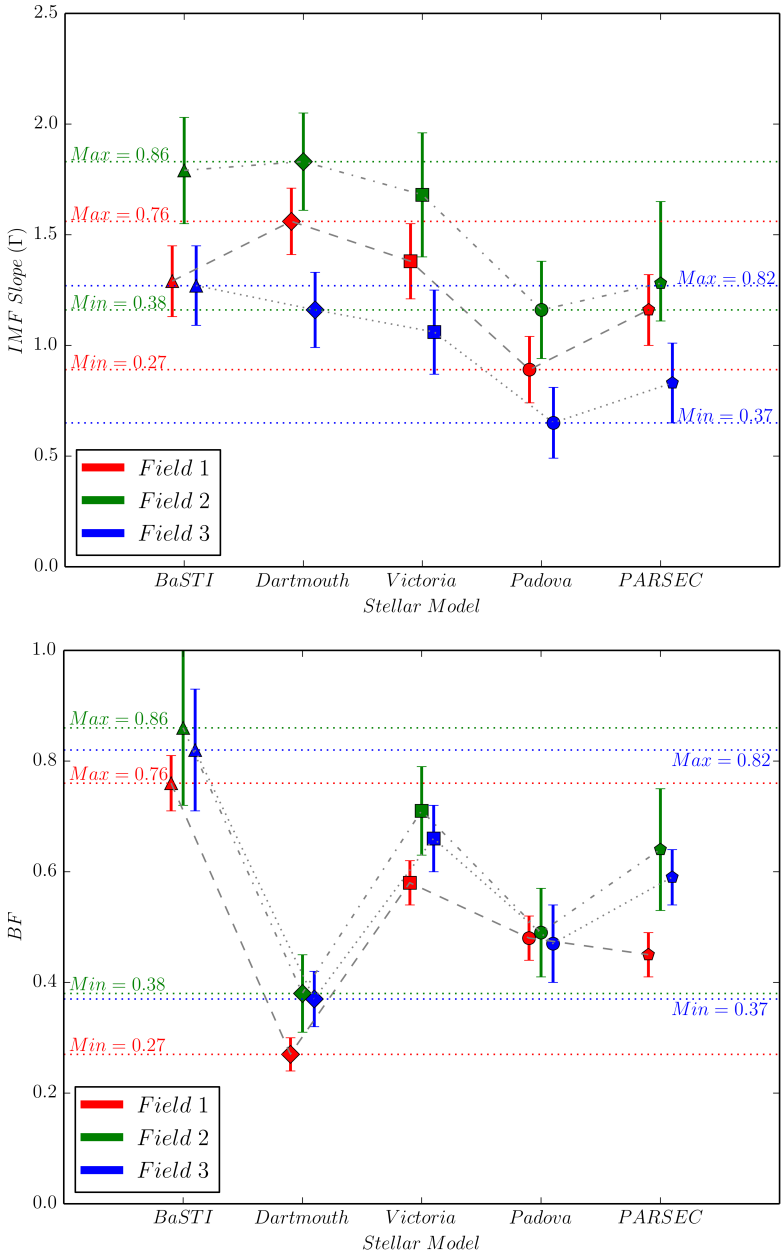

Figure 3.5 Stellar model dependence of the power-law IMF slope (left) and binary fraction (right). d is the mean galactocentric distance in parsecs. The values of the IMF slope and binary fraction in each field strongly depend on the utilized stellar library, suggesting that current knowledge of the lower-main sequence stars is uncertain. Literature IMF slopes are from Salpeter [1955], Kalirai et al. [2013] and Geha et al. [2013].

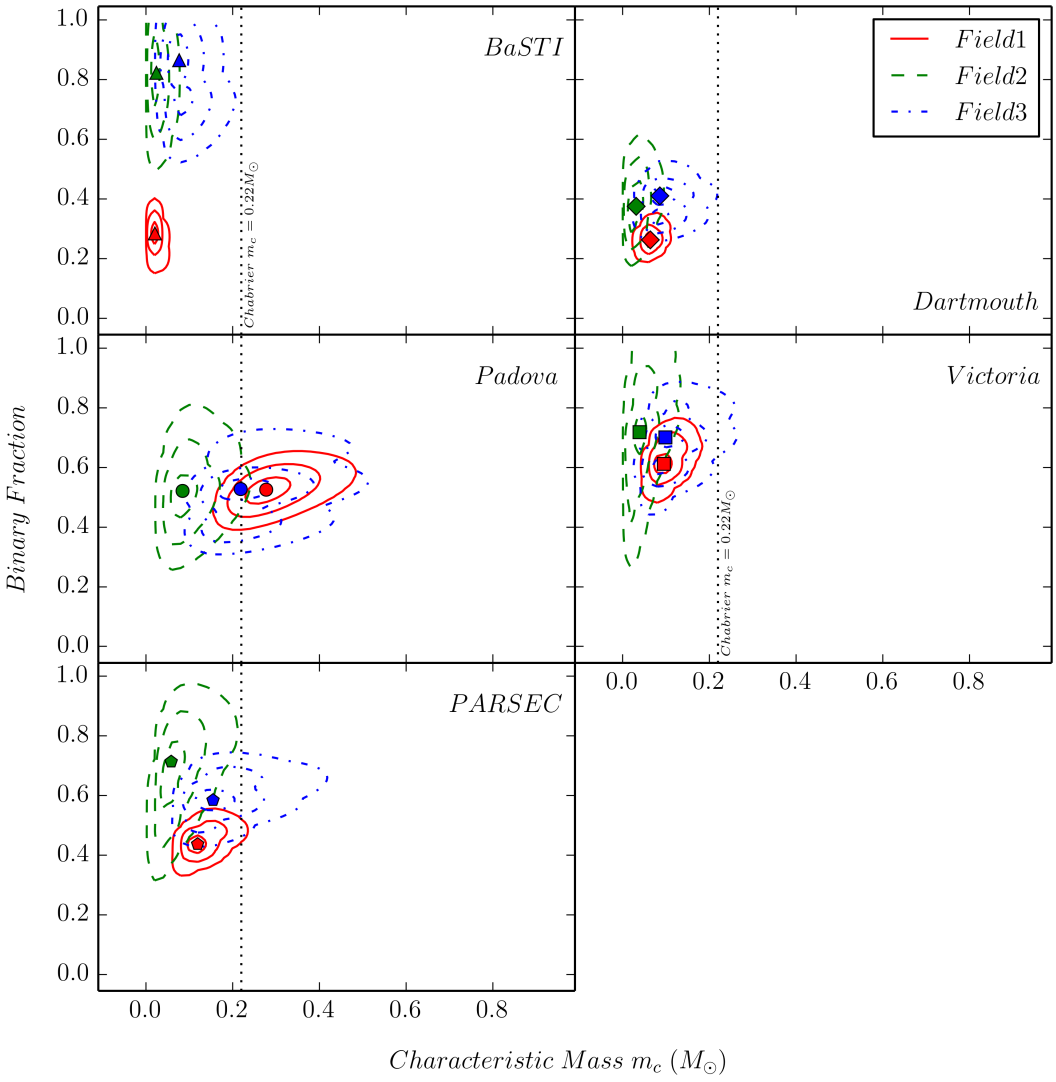

Figure 3.6 Log-normal IMF analysis. We are constraining the Characteristic mass (m_c) and Binary Fraction for $\sigma = 0.57$.

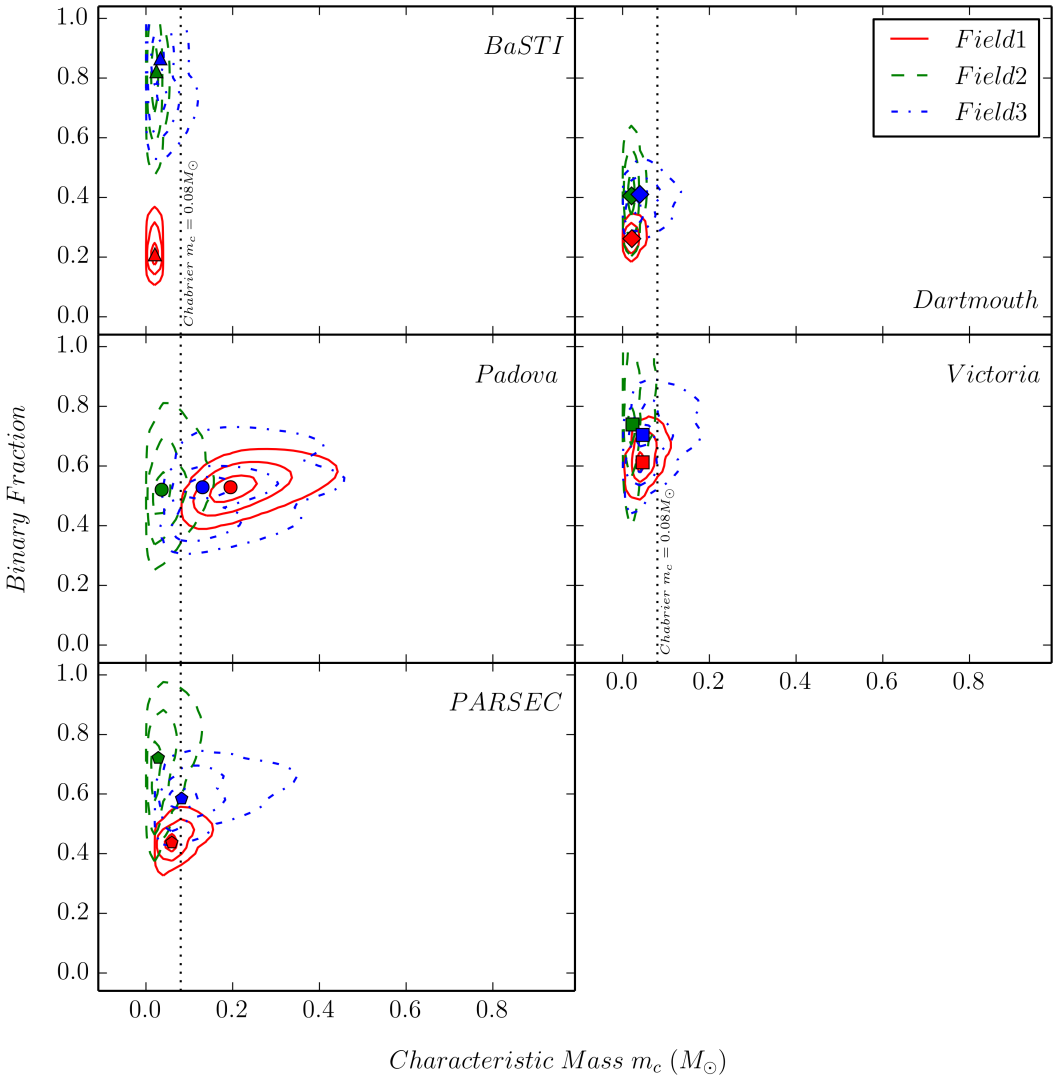

Figure 3.7 Log-normal IMF analysis. We are constraining the Characteristic mass (m_c) and Binary Fraction for $\sigma = 0.69$.

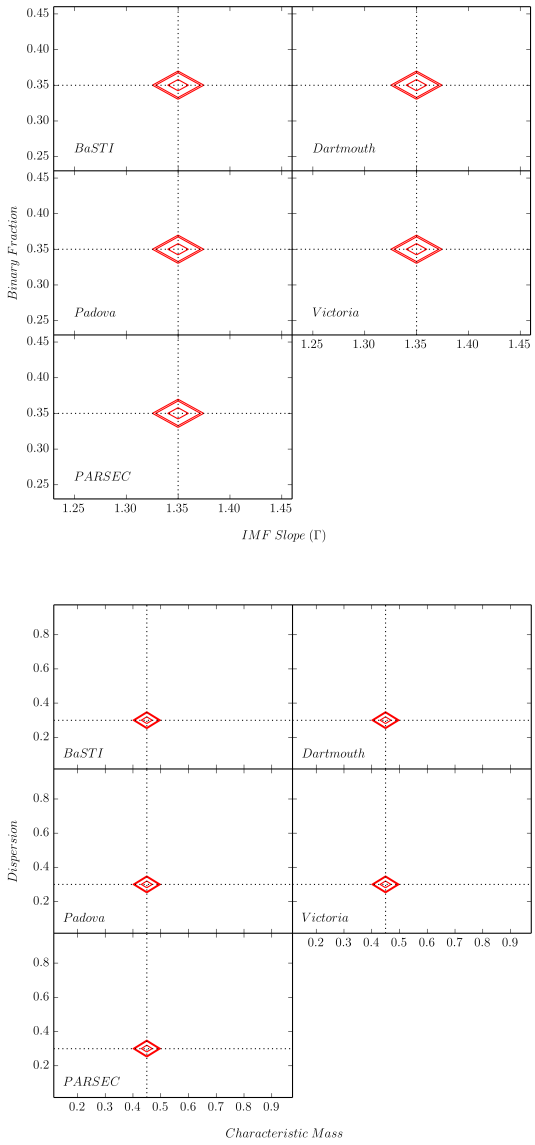

Figure 3.8 [top] Fitting a power-law IMF to a synthetic stellar population which is generated assuming a power-law IMF ($\Gamma = 1.35$) and a binary fraction of 0.35. Contours show up to a 3σ level. Very tight significance intervals show how reliable our analysis is. [bottom] Confidence contours for fitting a log-normal IMF to an artificial CMD which is generated based on a log-normal IMF ($\sigma = 0.30$ and $m_c = 0.45 M_\odot$) and a binary fraction of 0.35.

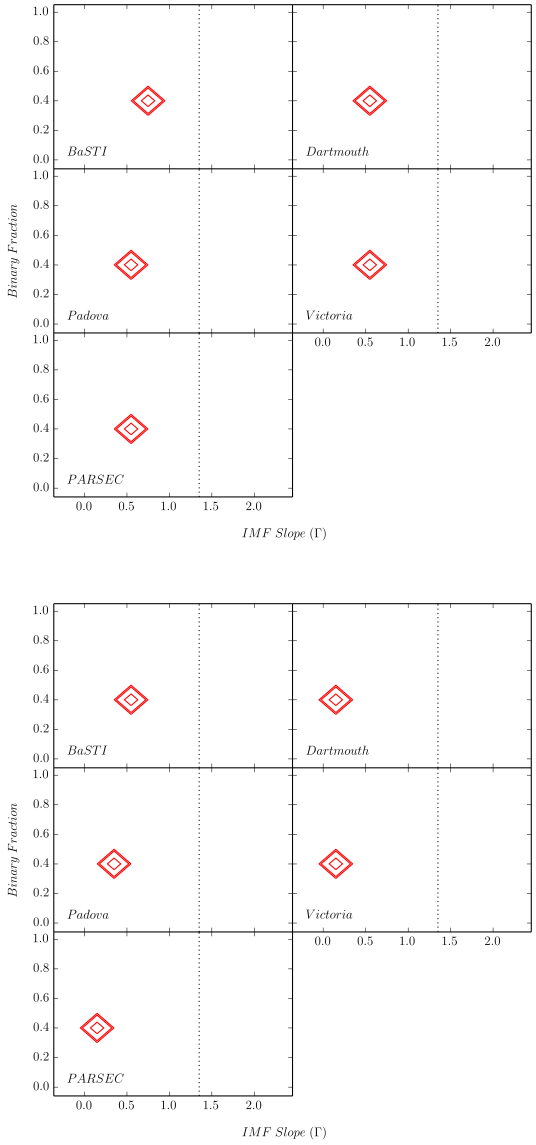

Figure 3.9 [top] Confidence contours for fitting a power-law IMF to an artificial CMD which is generated based on a log-normal IMF ($\sigma = 0.69$ and $m_c = 0.08 M_\odot$) and a binary fraction of 0.35. [bottom] Synthetic CMD has been created using a log-normal IMF ($\sigma = 0.57$ and $m_c = 0.22 M_\odot$) and a binary fraction of 0.35. Then, MATCH was run to fit a power-law IMF to the stellar population. All the stellar models agree upon a very similar Γ, at least at a 2σ confidence level. Dotted lines are showing the Salpeter IMF for reference.

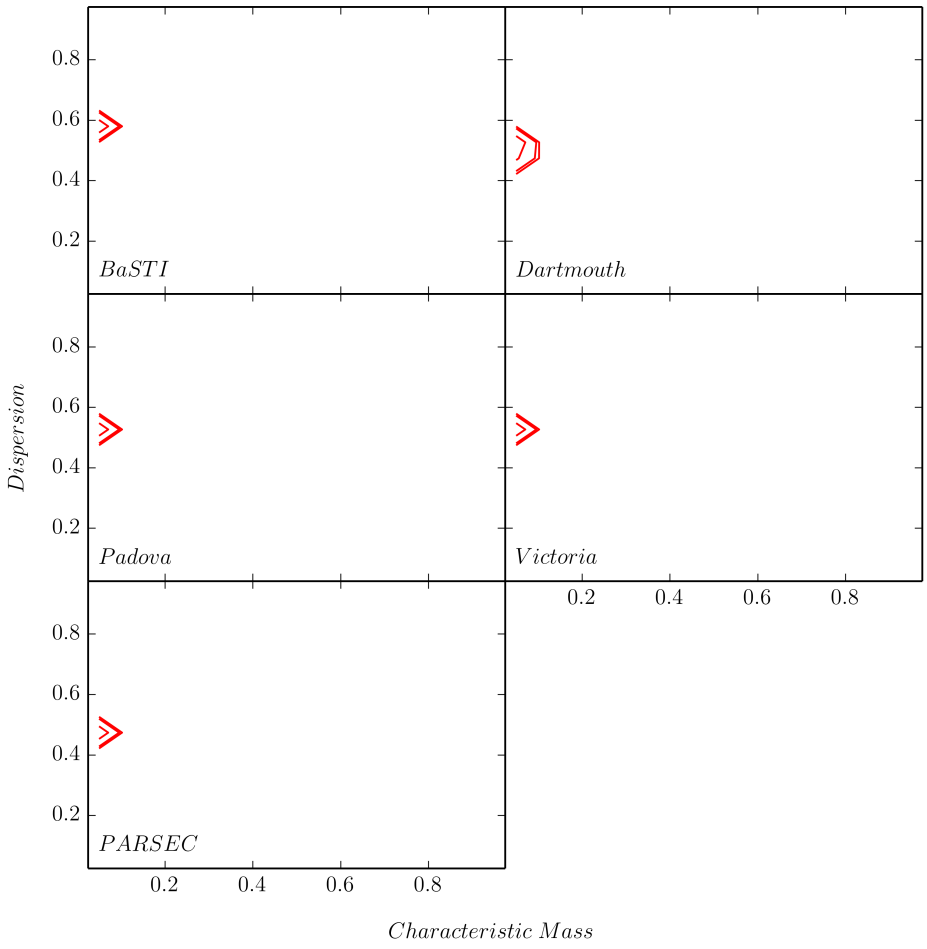

Figure 3.10 Confidence contours for fitting a log-normal IMF to an artificial CMD which is generated based on a power-law IMF ($\Gamma = 1.35$) and a binary fraction of 0.35.

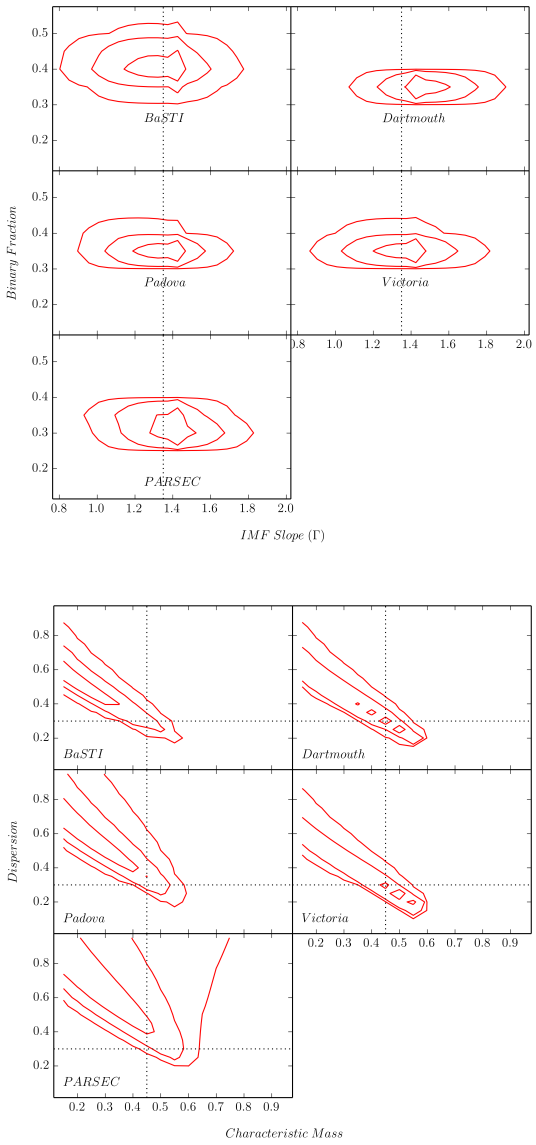

Figure 3.11 (Draco-like) [top] Confidence contours for fitting a power-law IMF to an artificial CMD which is generated based on a power-law IMF ($\Gamma = 1.35$) and a binary fraction of 0.35. [bottom] Confidence contours for fitting a log-normal IMF to an artificial CMD which is generated based on a log-normal IMF ($\sigma = 0.30$ and $m_c = 0.45 m_{\odot}$) and a binary fraction of 0.35.

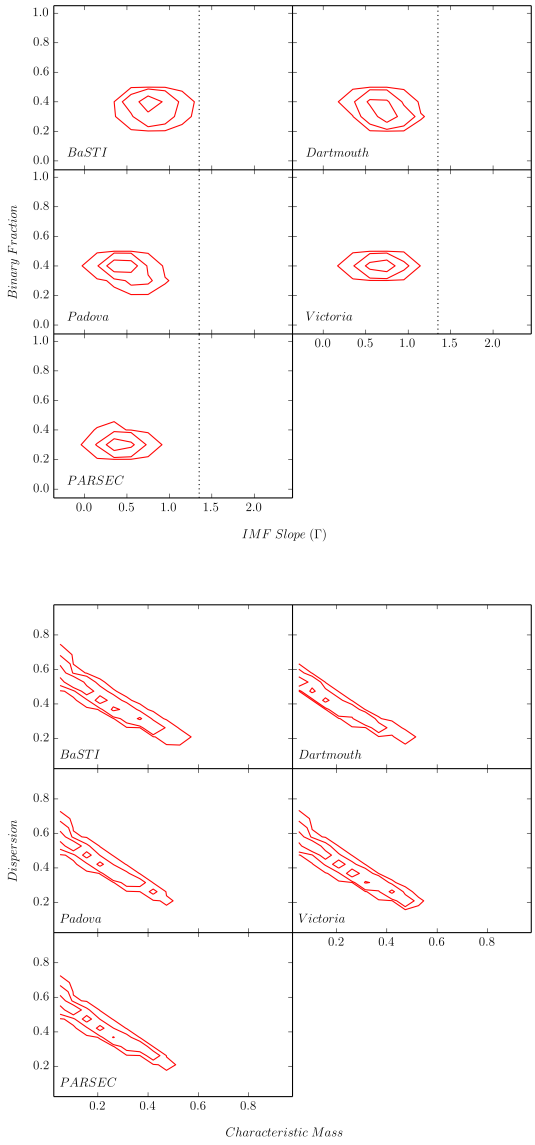

Figure 3.12 (Draco-like) [top] Confidence contours for fitting a power-law IMF to an artificial CMD which is generated based on a log-normal IMF ($\sigma = 0.30$ and $m_c = 0.45 m_\odot$) and a binary fraction of 0.35. [bottom] Confidence contours for fitting a log-normal IMF to an artificial CMD which is generated based on a power-law IMF ($\Gamma = 1.35$) and a binary fraction of 0.35.

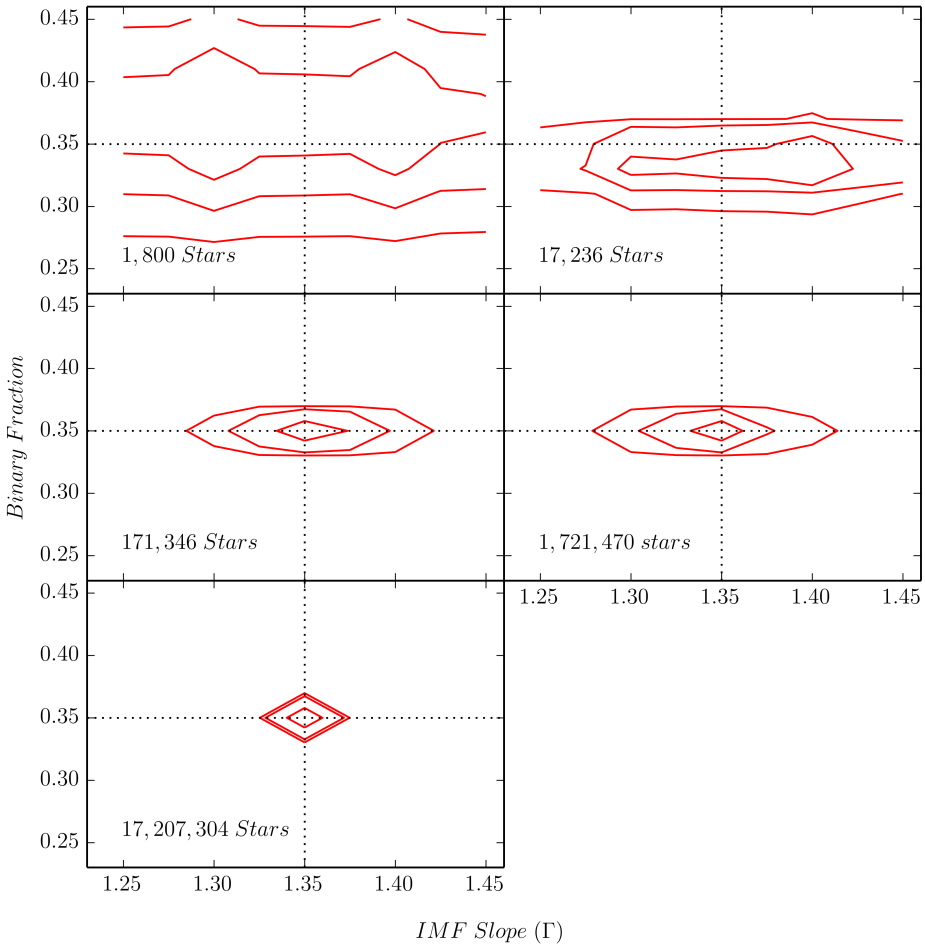

Figure 3.13 Confidence contours for fitting a power-law IMF to an artificial CMD which is generated based on a power-law IMF ($\Gamma = 1.35$) and a binary fraction of 0.35. Different panels correspond to different SFRs. Our SFR values are 10^{-5}, 10^{-4}, 10^{-3}, 10^{-2} and 10^{-1} solar mass/year.

Chapter 4

Summary and Conclusions

We have presented new analysis of the low-mas stellar initial mass function ($\sim$0.5-0.8$M_{\odot}$) in Local Group dwarf spheroidal galaxy Draco. Using archival HST/ACS and WFC3 optical imaging, we construct deep color-magnitude diagrams (CMD) at 3 different galactocentric radii and measure the IMF by modeling the resolved lower main sequence. We used five different stellar models (Padova, BaSTI, Dartmouth, Victoria and PARSEC) in our studies to see how adopted models can affect our results. For a single-sloped power-law IMF model, we find that the IMF slope steepens by up to $\sim$0.7 dex for radii between 150 and 300pc, while the binary fraction remains approximately constant. The absolute values of the IMF slopes at any radius depend strongly on the adopted stellar models, suggesting that current knowledge of the lower-main sequence stars is uncertain. Based on our results adopting different models can result in up to $\sim$ 0.67 dex difference in the IMF slope. We emphasize the importance of including variations in IMF slope measurements due to multiple stellar models as a means of estimating systematic uncertainties. Later, we presented two log-normal IMF solutions for our data by assuming two different values for the dispersion (σ). Because of our limited mass range, log-normal solutions with 3 free parameters are highly degenerate. Moreover, we presented detailed simulation studies of low-mass stellar IMF using MATCH to determine how reliable our studies of the IMF in Draco are. Based on our simulations, we're pretty confident that our IMF solutions are reliable and strongly rule out the need for a log-normal IMF to describe the low mass IMF in our three fields in Draco in the adopted mass range.

References

F. C. Adams and M. Fatuzzo. A Theory of the Initial Mass Function for Star Formation in Molecular Clouds. *ApJ*, 464:256, June 1996. doi: 10.1086/177318.

A. Aparicio, R. Carrera, and D. Martínez-Delgado. The Star Formation History and Morphological Evolution of the Draco Dwarf Spheroidal Galaxy. *AJ*, 122:2524–2537, November 2001. doi: 10.1086/323535.

N. Bastian, K. R. Covey, and M. R. Meyer. A Universal Stellar Initial Mass Function? A Critical Look at Variations. *ARA&A*, 48:339–389, September 2010. doi: 10.1146/annurev-astro-082708-101642.

M. R. Bate. The importance of radiative feedback for the stellar initial mass function. *MNRAS*, 392:1363–1380, February 2009. doi: 10.1111/j.1365-2966.2008.14165.x.

M. Bellazzini, F. R. Ferraro, L. Origlia, E. Pancino, L. Monaco, and E. Oliva. The Draco and Ursa Minor Dwarf Spheroidal Galaxies: A Comparative Study. *AJ*, 124: 3222–3240, December 2002. doi: 10.1086/344794.

H. Bouy, W. Brandner, E. L. Martín, X. Delfosse, F. Allard, and G. Basri. Multiplicity of Nearby Free-Floating Ultracool Dwarfs: A Hubble Space Telescope WFPC2 Search for Companions. *AJ*, 126:1526–1554, September 2003. doi: 10.1086/377343.

A. Bressan, P. Marigo, L. Girardi, B. Salasnich, C. Dal Cero, S. Rubele, and A. Nanni. PARSEC: stellar tracks and isochrones with the PAdova and TRieste Stellar Evolution Code. *MNRAS*, 427:127–145, November 2012. doi: 10.1111/j.1365-2966.2012.21948.x.

G. Chabrier. Galactic Stellar and Substellar Initial Mass Function. *PASP*, 115:763–795, July 2003. doi: 10.1086/376392.

K. R. Covey, M. A. Agüeros, P. J. Green, D. Haggard, W. A. Barkhouse, J. Drake, N. Evans, V. Kashyap, D.-W. Kim, A. Mossman, D. O. Pease, and J. D. Silverman. The ChaMP Extended Stellar Survey (ChESS): Photometric and Spectroscopic Properties of Serendipitously Detected Stellar X-Ray Sources. *ApJS*, 178:339-358, October 2008. doi: 10.1086/590909.

G. de Marchi, F. Paresce, and S. Portegies Zwart. The stellar IMF of galactic clusters and its evolution. In E. Corbelli, F. Palla, and H. Zinnecker, editors, *The Initial Mass Function 50 Years Later*, volume 327 of *Astrophysics and Space Science Library*, page 77, January 2005.

A. E. Dolphin. WFPC2 Stellar Photometry with HSTPHOT. *PASP*, 112:1383–1396, October 2000. doi: 10.1086/316630.

A. E. Dolphin. Numerical methods of star formation history measurement and applications to seven dwarf spheroidals. *MNRAS*, 332:91–108, May 2002. doi: 10.1046/j.1365-8711.2002.05271.x.

A. Dotter, B. Chaboyer, D. Jevremović, V. Kostov, E. Baron, and J. W. Ferguson. The Dartmouth Stellar Evolution Database. *ApJS*, 178:89–101, September 2008. doi: 10.1086/589654.

A. Duquennoy and M. Mayor. Multiplicity among solar-type stars in the solar neighbourhood. II - Distribution of the orbital elements in an unbiased sample. *A&A*, 248: 485–524, August 1991.

B. G. Elmegreen and J. Scalo. The Effect of Star Formation History on the Inferred Stellar Initial Mass Function. *ApJ*, 636:149–157, January 2006. doi: 10.1086/497889.

D. A. Fischer and G. W. Marcy. Multiplicity among M dwarfs. *ApJ*, 396:178–194, September 1992. doi: 10.1086/171708.

M. Geha, T. M. Brown, J. Tumlinson, J. S. Kalirai, J. D. Simon, E. N. Kirby, D. A. VandenBerg, R. R. Muñoz, R. J. Avila, P. Guhathakurta, and H. C. Ferguson. The Stellar Initial Mass Function of Ultra-faint Dwarf Galaxies: Evidence for IMF Variations with Galactic Environment. *ApJ*, 771:29, July 2013. doi: 10.1088/0004-637X/771/1/29.

L. Girardi, B. F. Williams, K. M. Gilbert, P. Rosenfield, J. J. Dalcanton, P. Marigo, M. L. Boyer, A. Dolphin, D. R. Weisz, J. Melbourne, K. A. G. Olsen, A. C. Seth, and E. Skillman. The ACS Nearby Galaxy Survey Treasury. IX. Constraining Asymptotic Giant Branch Evolution with Old Metal-poor Galaxies. *ApJ*, 724:1030–1043, December 2010. doi: 10.1088/0004-637X/724/2/1030.

J. S. Kalirai, J. Anderson, A. Dotter, H. B. Richer, G. G. Fahlman, B. M. S. Hansen, J. Hurley, I. N. Reid, R. M. Rich, and M. M. Shara. Ultra-Deep Hubble Space Telescope Imaging of the Small Magellanic Cloud: The Initial Mass Function of Stars with M. *ApJ*, 763:110, February 2013. doi: 10.1088/0004-637X/763/2/110.

E. N. Kirby, J. G. Cohen, P. Guhathakurta, L. Cheng, J. S. Bullock, and A. Gallazzi. The Universal Stellar Mass-Stellar Metallicity Relation for Dwarf Galaxies. *ApJ*, 779: 102, December 2013. doi: 10.1088/0004-637X/779/2/102.

J. T. Kleyna, M. I. Wilkinson, N. W. Evans, and G. Gilmore. First Clear Signature of an Extended Dark Matter Halo in the Draco Dwarf Spheroidal. *ApJ*, 563:L115–L118, December 2001. doi: 10.1086/338603.

P. Kroupa. On the variation of the initial mass function. *MNRAS*, 322:231–246, April 2001. doi: 10.1046/j.1365-8711.2001.04022.x.

P. Kroupa, C. A. Tout, and G. Gilmore. The distribution of low-mass stars in the Galactic disc. *MNRAS*, 262:545–587, June 1993. doi: 10.1093/mnras/262.3.545.

C. J. Lada. Stellar Multiplicity and the Initial Mass Function: Most Stars Are Single. *ApJ*, 640:L63–L66, March 2006. doi: 10.1086/503158.

R. B. Larson. A simple probabilistic theory of fragmentation. *MNRAS*, 161:133, 1973. doi: 10.1093/mnras/161.2.133.

R. B. Larson. Thermal physics, cloud geometry and the stellar initial mass function. *MNRAS*, 359:211–222, May 2005. doi: 10.1111/j.1365-2966.2005.08881.x.

J. Maíz Apellániz. Biases on Initial Mass Function Determinations. II. Real Multiple Systems and Chance Superpositions. *ApJ*, 677:1278-1295, April 2008. doi: 10.1086/533525.

P. Marigo, L. Girardi, A. Bressan, M. A. T. Groenewegen, L. Silva, and G. L. Granato. Evolution of asymptotic giant branch stars. II. Optical to far-infrared isochrones with improved TP-AGB models. *A&A*, 482:883–905, May 2008. doi: 10.1051/0004-6361:20078467.

B. D. Mason, W. I. Hartkopf, D. R. Gies, T. J. Henry, and J. W. Helsel. The High Angular Resolution Multiplicity of Massive Stars. *AJ*, 137:3358–3377, February 2009. doi: 10.1088/0004-6256/137/2/3358.

M. L. Mateo. Dwarf Galaxies of the Local Group. *ARA&A*, 36:435–506, 1998. doi: 10.1146/annurev.astro.36.1.435.

G. E. Miller and J. M. Scalo. The initial mass function and stellar birthrate in the solar neighborhood. *ApJS*, 41:513–547, November 1979. doi: 10.1086/190629.

A. T. Myers, M. R. Krumholz, R. I. Klein, and C. F. McKee. Metallicity and the Universality of the Initial Mass Function. *ApJ*, 735:49, July 2011. doi: 10.1088/0004-637X/735/1/49.

S. Nayakshin and M. I. Wilkinson. A link between feedback outflows and satellite galaxy suppression. *MNRAS*, 433:324–331, July 2013. doi: 10.1093/mnras/stt724.

M. S. Pawlowski and P. Kroupa. The rotationally stabilized VPOS and predicted proper motions of the Milky Way satellite galaxies. *MNRAS*, 435:2116–2131, November 2013. doi: 10.1093/mnras/stt1429.

A. Pietrinferni, S. Cassisi, M. Salaris, and F. Castelli. A Large Stellar Evolution Database for Population Synthesis Studies. I. Scaled Solar Models and Isochrones. *ApJ*, 612:168–190, September 2004. doi: 10.1086/422498.

E. E. Salpeter. The Luminosity Function and Stellar Evolution. *ApJ*, 121:161, January 1955. doi: 10.1086/145971.

J. M. Scalo. The stellar initial mass function. *Fund. Cosmic Phys.*, 11:1–278, May 1986.

S. T. Sohn, G. Besla, R. P. van der Marel, M. Boylan-Kolchin, S. R. Majewski, and J. S. Bullock. The Space Motion of Leo I: Hubble Space Telescope Proper Motion and Implied Orbit. *ApJ*, 768:139, May 2013. doi: 10.1088/0004-637X/768/2/139.

D. A. VandenBerg, P. A. Bergbusch, and P. D. Dowler. The Victoria-Regina Stellar Models: Evolutionary Tracks and Isochrones for a Wide Range in Mass and Metallicity that Allow for Empirically Constrained Amounts of Convective Core Overshooting. *ApJS*, 162:375–387, February 2006. doi: 10.1086/498451.

D. R. Weisz, A. E. Dolphin, E. D. Skillman, J. Holtzman, K. M. Gilbert, J. J. Dalcanton, and B. F. Williams. The Star Formation Histories of Local Group Dwarf Galaxies. I. Hubble Space Telescope/Wide Field Planetary Camera 2 Observations. *ApJ*, 789: 147, July 2014. doi: 10.1088/0004-637X/789/2/147.

H. Zinnecker. Star formation from hierarchical cloud fragmentation - A statistical theory of the log-normal Initial Mass Function. *MNRAS*, 210:43–56, September 1984. doi: 10.1093/mnras/210.1.43.

H. Zinnecker and H. W. Yorke. Toward Understanding Massive Star Formation. *ARA&A*, 45:481–563, September 2007. doi: 10.1146/annurev.astro.44.051905.092549.